Optimization of the Composition of PdAuCu Ternary Alloy Nanoparticles for Plasmonic Hydrogen Sensing

N.B. When citing this work, cite the original published paper.

(article starts on next page)

Article

Optimization of the Composition of PdAuCu Ternary Alloy Nanoparticles for Plasmonic Hydrogen Sensing

Iwan Darmadi, Sarah Zulfa Khairunnisa, David Tomeček, and Christoph Langhammer*

Read Online

ACCESS | Metrics & More | Article Recommendations

ABSTRACT: Alloying is a long-standing central strategy in materials science for the tailoring and optimization of bulk material properties, which more recently has started to find application also in engineered nanomaterials and nanostructures used in, among other, nanoplasmonic hydrogen sensors. Specifically, alloying Pd nanoparticles to form binaries and ternaries with the coinage metals Au and Cu has proven efficient to mitigate hysteresis in the sensor response, improve response and recovery times, boost sensitivity in the low hydrogen concentration sensing range, and reduce the detrimental impact of carbon monoxide poisoning. However, when surveying the corresponding studies, it is clear that there is a trade-off between the sensitivity enhancement and the CO-poisoning resistance effects provided by Au and Cu alloyants, respectively. Therefore, in this work, we systematically screen the impact of the Au and Cu concentration in PdAuCu ternary alloy nanoparticles used for plasmonic hydrogen sensing, to obtain a champion system with maximized sensitivity and CO-poisoning resistance based on an evaluation using the stringent ISO 26142 test protocol. As the main results, we find that the best hysteresis-free and sensitive response combined with deactivation resistance to 500 ppm CO in synthetic air is obtained for the $Pd_{65}Au_{25}Cu_{10}$ ternary alloy system, which also exhibits good long-term stability during operation under severe CO poisoning conditions.

KEYWORDS: ternary alloy, plasmonic hydrogen sensing, hydrogen, CO, poisoning, hysteresis, palladium, gold, copper
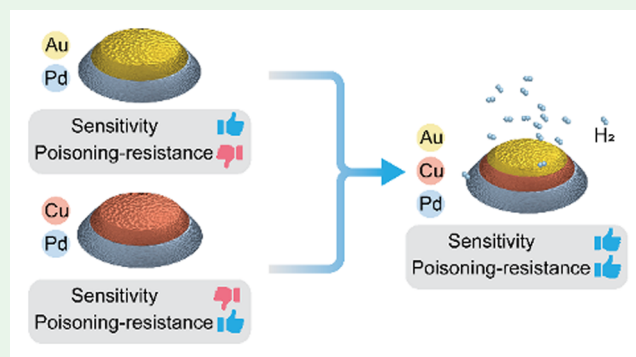
INTRODUCTION

The development of hydrogen safety sensors has accelerated significantly in recent years due to the imminent large-scale implementation of hydrogen-energy technologies. Among the emerging hydrogen sensor principles, solutions based on nanosized Pd and optical readout based on localized surface plasmon resonance (LSPR) are among the most promising and mature ones.[1] Such nanoplasmonic hydrogen sensors rely on visible light-induced collective and coherent excitation of electrons in hydride-forming metal nanoparticles—the LSPR—as a signal transducing mechanism, where the hydrogen sorption and hydride formation processes give rise to a sizable optical contrast, which is proportional to the hydrogen concentration in the sensor surroundings.[2] At the same time, despite their excellent selectivity toward hydrogen gas, the performance of pure Pd-based sensors, in general, and of plasmonic solutions, in particular, is hampered by several inherent limitations, such as hysteresis, slow response/recovery times, and proneness to deactivation by poisoning species like CO.[2−5] As a consequence, numerous strategies have been developed to minimize the impact of these negative effects and the use of coinage metal-Pd alloys has emerged as one of the most promising directions in this respect.[6−10] For example,

hydride formation hysteresis can be suppressed by alloying Pd nanoparticles with at least 25 at % Au.[7,11] Interestingly, the corresponding research also has revealed that alloying with Au reduces the hydrogen sorption apparent activation energies, which leads to faster sensor response/recovery compared to pure Pd.[12] Similarly, it has been demonstrated that also a second limitation of pure Pd can be mitigated by alloying since the addition of Cu to Pd significantly improves the resistance against sensor poisoning and deactivation by CO.[8,10] Following this line, in a proof-of-principle fashion, we have recently shown that these two strategies can be combined in a ternary PdAuCu alloy for plasmonic optical hydrogen detection.[10] However, in such a ternary system, the introduction of Cu not only mitigates the CO poisoning effect but also quite dramatically reduces sensor sensitivity due to the shift of the two-phase equilibrium plateau to higher hydrogen partial

A

pressures.[13,14] Therefore, to optimize the performance of this ternary alloy system for application in plasmonic hydrogen sensors, there is an imminent demand for the systematic optimization of the alloy components with respect to the following three criteria: (i) poisoning/deactivation resistance, (ii) hysteresis suppression, and (iii) sensitivity. Therefore, here, we systematically screen the impact of the ternary PdAuCu alloy composition on these three parameters, and we implement for the first time in plasmonic hydrogen sensor evaluation the rigorous ISO 26142 testing protocol recommended by the US National Renewable Energy Laboratory (NREL) to assess sensor poisoning and deactivation under simulated application conditions in synthetic air.[15]

■ RESULTS AND DISCUSSION

To determine the minimal amount of Cu required to obtain a sizable CO-poisoning protection, we first systematically investigated binary PdCu nanoparticle arrays fabricated using hole-mask colloidal lithography[16,17] (Figure 1a) and comprised
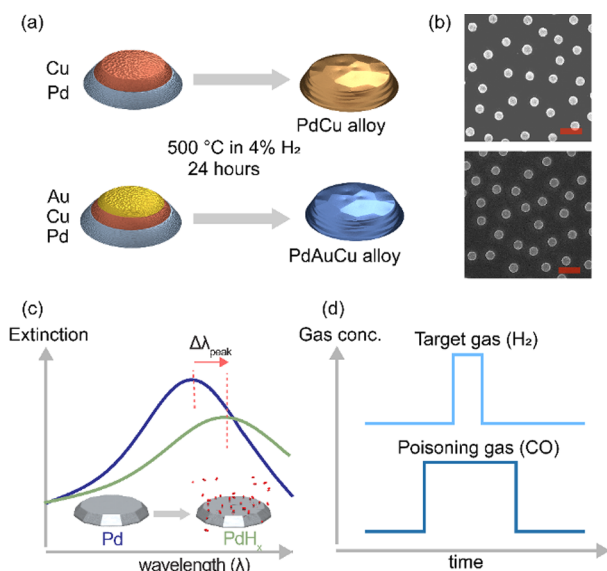

Figure 1. (a) Schematic of PdCu and PdAuCu alloy nanoparticle fabrication. The alloy composition is adjusted by tuning the thickness of the corresponding layers evaporated through the hole mask.[17] Subsequently, a homogeneous alloy is obtained by annealing at 500 °C in 4% H_2 + 96% Ar for 24 h.[10,11] (b) SEM micrograph of a representative $Pd_{90}Cu_{10}$ (top) and $Pd_{65}Au_{25}Cu_{10}$ (bottom) alloy nanodisk quasi-random array. Scale bar 500 nm. (c) Schematic of the plasmonic sensing readout. The sensor response is defined as the plasmonic peak shift ($\Delta\lambda_{peak}$) of the Pd(alloy) nanoparticles during the hydrogen absorption/desorption. (d) Schematic of the test protocol used to assess CO poisoning tolerance according to ISO 26142.

of quasi-random arrangements of nanodisks with an average diameter of 190 nm and a height of 25 nm (Figure 1b). The alloy at. % composition was adjusted by controlling the thickness of the evaporated constituent layers. Later, the multilayer nanodisks were annealed at 500 °C in 4% H_2 + 96% Ar for 24 h to ensure complete alloy formation through the particles.[10] Specifically, we nanofabricated a series of PdCu alloy samples with Cu concentrations of 0, 1, 3, 5, 7, 10, and 15 at. %. We then evaluated their optical plasmonic response, defined as spectral peak-centroid position shifts,[18] $\Delta\lambda_{peak}$ (Figure 1c), to 3 vol. % H_2 pulses in synthetic air (chosen as

a representative concentration close to the lower flammability limit of H_2 in air), and in CO backgrounds ranging from 100 to 500 ppm. Here, we highlight that the experiment was designed to comply with the ISO 26142 testing protocol[15] according to which the poisoning gas (CO) is introduced before the test gas pulse (H_2) and kept as a constant background in synthetic air (Figure 1d).

Focusing first on the response of the neat Pd control, we notice the severe impact of CO on the H_2 sorption kinetics, as signified by the $\Delta\lambda_{peak}$ signal not reaching saturation within the given 5 min of the H_2 pulse even at the lowest 100 ppm CO concentration (Figure 2). Also, the sensor does not recover within 5 min of a subsequent synthetic air carrier gas flush with 100 ppm CO. Furthermore, we see that there is a CO concentration dependence of the hydrogen absorption kinetics, with the response being fastest for the 100 ppm CO background. Similarly, we observe faster and more complete recovery of the sensor and a lower CO concentration in the gas. This implies a CO-concentration-dependent poisoning effect, which is reasonable since CO adsorption on Pd is expected to increase at a higher concentration according to, for instance, the Langmuir adsorption model.[19] Similarly, when the CO background is removed again, the sorption kinetics become faster, which indicates that the CO poisoning is not permanent, in agreement with an O_2-assisted reaction and desorption mechanism.[20]

To start the analysis of the impact of Cu concentration in the alloy nanoparticles on the CO poisoning resistance, we first glance over the response curves of the sensors with increasing Cu concentrations summarized in Figure 2. As a clear general trend, we see that the higher the Cu concentration, the more tolerant the sensor becomes to the presence of CO. Interestingly, in 100 ppm CO, as little as 1 at. % Cu is sufficient to remedy the CO poisoning significantly. These very low required Cu concentrations are somewhat surprising at first but can be rationalized on the basis of first-principles calculations, which show that CO binds less strongly on PdCu alloy surfaces compared to pure Pd, due to both an electronic ligand effect and a geometrical (ensemble) effect.[21−24] The ensemble effect in this case means that alloying reduces the number of three-Pd atom sites to which CO binds very strongly and that already rather small amounts of Cu on the surface are enough to the significantly reduce the availability of such sites.[25] Furthermore, the ensemble effect may even be more dominant if any surface segregation would occur since Cu is known to have a tendency to move to the surface.[26,27] Finally, we also note that it is plausible that Cu alloying also reduces the poisoning effect of sulfuric compounds (e.g. SO_2 and H_2S) since their adsorption mechanism is similar to the one of CO.[28,29]

For a more detailed analysis of the data presented in Figure 2 and to investigate the minimum Cu concentration required to achieve significant CO tolerance, we focus on the sensor response during the first hydrogen cycle in the five different CO background concentrations at hand (Figure 3a−d). This analysis reveals both a decreasing steady state $\Delta\lambda_{peak}$ for increasing Cu concentration (see detailed discussion below) and a pronounced CO poisoning effect for H_2 desorption manifested as the deceleration of the kinetics. For absorption, we cannot properly resolve the true kinetics since the gas exchange time constant of the used flow reactor system is similar to the response time of the sensor. Therefore, we used the temporal response of the sensors during (the significantly
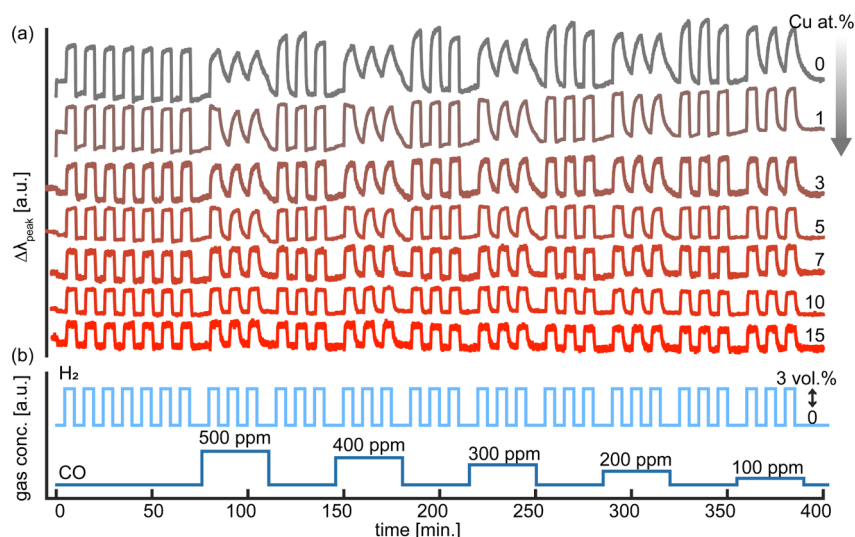
Figure 2. (a) Temporal evolution of the optical response, $\Delta\lambda_{peak}$, for PdCu alloy nanoparticles with different Cu contents of 1, 3, 5, 7, 10, and 15 at. % during (b) 3 vol. % H_2 pulses in varying CO backgrounds in synthetic air carrier gas. The tests were done at 30 °C.
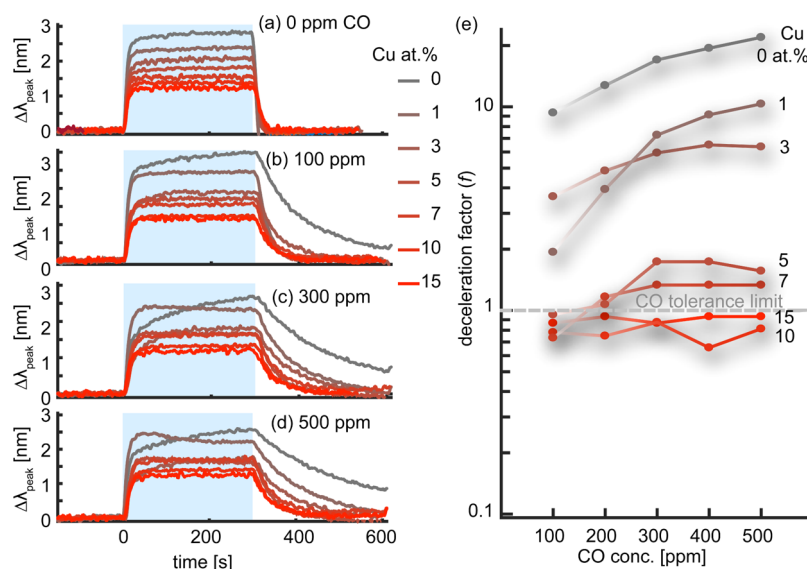

Figure 3. Temporal $\Delta\lambda_{peak}$ response of PdCu binary alloys with Cu = 0, 1, 3, 5, 7, 10, and 15 at. % concentrations to 3 vol. % H_2 pulses (blue-shaded areas) in synthetic air and in CO background concentrations of (a) 0 ppm, (b) 100 ppm, (c) 300 ppm, and (d) 500 ppm. (e) CO deceleration factor, f, obtained by comparing the desorption kinetics with and without the CO background in synthetic air.

slower) hydrogen desorption to quantitatively analyze the effect of Cu for increasing CO tolerance. Moreover, the deceleration effect of CO is more apparent in the desorption process because the rate-limiting factor for desorption is hydrogen recombination on the Pd surface,[30,31] which is more susceptible to CO poisoning. In contrast, the absorption process is rate-limited by hydrogen diffusion in the Pd bulk.[32]

We define the CO deceleration factor as

$$f = \frac{t_{50}^{CO} - t_{50}}{t_{50}}$$

where t_{50} is the time to reach 50% of the full signal for a H_2 concentration change in pure synthetic air.[33] The CO superscript in t_{50}^{CO} denotes t_{50} measured in the CO background. With this definition, the deceleration factor, f, reflects the sensor tolerance to CO poisoning, where a larger f indicates reduced CO tolerance. The correspondingly derived deceler-

ation factors of all alloys for different CO concentrations are plotted in Figure 3e. If we then set the tolerance limit to $f = 1$, only the 10 and 15 at. % Cu alloys can be considered CO tolerant up to 500 ppm CO. This indicates that the required Cu concentration to promote CO resistance is higher than that we previously reported (5 at. %),[10] as a consequence of the more rigorous evaluation in the ISO 26142 framework used here, and that it strongly depends on the absolute CO concentration in the background. Hence, for our further optimization of the ternary PdAuCu alloy system reported below, we use ≥10 at. % Cu. Finally, we also note that the identified deactivation resistance is quite remarkable, considering that the CO background concentration implemented in ISO 26142 tests of commercial sensors was one order of magnitude lower, that is, 50 ppm.[34]

Having identified the necessary minimal Cu content in a Pd alloy for achieving a sizable CO-poisoning resistance in the ISO 26142 testing protocol, we now turn to assess the impact

C

of adding Au to the PdCu system with respect to obtaining hysteresis-free response and maximized sensitivity. For this purpose, we first measured optical $\Delta\lambda_{peak}$ isotherms at 30 °C in a custom-built vacuum chamber with optical access.[7] We used samples alloyed with 10, 15, and 20 at. % Cu, respectively, to which we added 15, 20, 25, and 30 at. % Au to form the corresponding ternary systems (Figure 4). This analysis shows
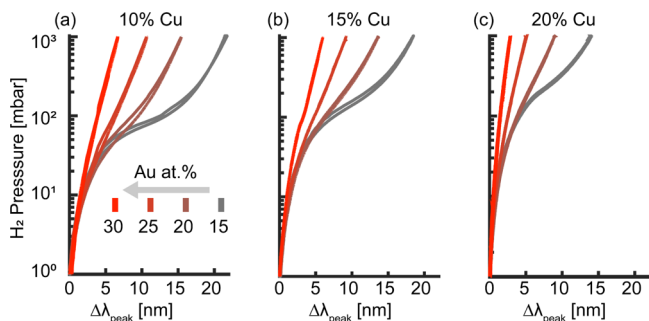

Figure 4. Pressure−$\Delta\lambda_{peak}$ isotherms for PdAuCu ternary alloys with different constant Cu concentrations. Each panel depicts alloys with a constant Cu concentration of (a) 10 at. %, (b) 15 at. %, and (c) 20 at. %, for a Au content systematically varying from 15−30 at. %. Note the smaller amount of Au necessary for complete hysteresis suppression for a higher Cu content in the alloy.

that for 10 at. % Cu, at least 30 at. % Au is necessary for complete hysteresis suppression (Figure 4a). For 15 at. % Cu, complete suppression is achieved with 25 at. % Au (Figure 4b), and for 20 at. % Cu, only 20 at. % Au is necessary (Figure 4c). Therefore, complete hysteresis suppression is achieved when the sum of Au and Cu is around 40 at. %, which is slightly higher than the necessary concentration in binary PdAu alloys, where complete hysteresis suppression is achieved at 30 at. % Au.[7,35,36] This implies that, to some extent in the ternary system, Au and Cu are annulling each other with respect to the hysteresis suppression effect because Au expands the host lattice[37] and Cu contracts it[38] due to larger and smaller atomic radii, respectively, compared to the Pd host.

To provide a different perspective of the data shown in Figure 4, we replot the same isotherms but for a constant Au concentration in each panel (Figure 5). Starting with 15 at. % Au and three Cu concentrations of 10, 15, and 20 at. %, we clearly see how the addition of Cu elevates the plateau pressure of the ternary system in the same way as observed for PdCu binaries (Figure 5a).[10] The same trend can also be found for ternaries based on 20, 25, and 30 at. % Au (Figure 5b−d). Simultaneously, increasing the Cu concentration also induces a significant reduction in $\Delta\lambda_{peak}$ for a given hydrogen pressure change (Figure 5), which is equivalent to a sizable reduction of sensor sensitivity and thus limit of detection.

In summary, the data presented in Figures 4 and 5 indicate that in PdAuCu ternary alloys, Au mainly contributes to the closing of the hysteresis gap, whereas Cu leads to an elevation of the plateau region to higher hydrogen partial pressures. Projected onto the hydrogen sensor application, this means that there exists an optimal ternary alloy composition which is the best compromise between the pros and cons of alloying with Au and Cu, with respect to (i) eliminating the hysteresis gap and (ii) maximizing the magnitude of $\Delta\lambda_{peak}$ per hydrogen partial pressure change. Criterion (i) is achieved for alloys with at least 25 at. % Au, and criterion (ii) sets an upper limit to both Au and Cu concentrations since increasing them
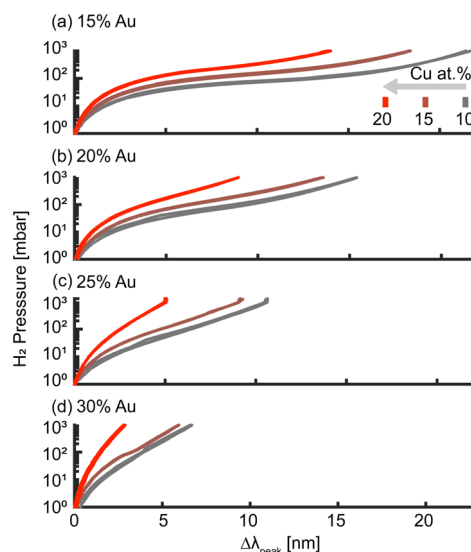

Figure 5. Pressure−$\Delta\lambda_{peak}$ isotherms for PdAuCu ternary alloys with different constant Au concentrations. Each panel depicts alloys with constant Au concentrations of (a) 15 at. %, (b) 20 at. %, (c) 25 at. %, and (d) 30 at. % for a Cu content systematically varying from 10−20 at. %. Note the significantly reduced magnitude of $\Delta\lambda_{peak}$ for a given hydrogen pressure change as both Cu and Au contents are increased.

generically reduces the overall sensor sensitivity because $\Delta\lambda_{peak}$ per hydrogen partial pressure change is reduced. As the result of these selection rules, the $Pd_{65}Au_{25}Cu_{10}$ ternary alloy system emerges as the best compromise and thus our champion system. It is worth mentioning that the slight gap between the absorption and desorption branches observed for the $Pd_{65}Au_{25}Cu_{10}$ alloy in Figure 5c is a measurement artifact rather than an inherent hydride hysteresis gap. This is corroborated by the absence of the $\alpha-\beta$ phase transition along the curve, which is a strong indication of hysteresis-free hydride formation.

As the last step of our analysis, we therefore investigate the poisoning resistance of $Pd_{65}Au_{25}Cu_{10}$ by exposing it to more than 50 five-minute pulses of 4 vol. % H_2 in the constant 500 ppm CO background in synthetic air carrier gas at 30 °C, over a duration of 12 h (Figure 6a,b). Evidently, the sensor exhibits excellent stability and deactivation resistance, as manifested in essentially constant response and recovery times (Figure 6c) during the entire experiment. Furthermore, response/recovery times are identical to those of the sensor operating in pure synthetic air (no CO background) both before and after CO exposure and in 500 ppm CO. The $\Delta\lambda_{peak}$ amplitude (Figure 6d), on the other hand, shows a slight drift, which may indicate a minor gradual change that is likely due to alloyant surface segregation within the first few atomic layers, induced by CO and O_2.[39−42] The overall nanodisk shape and arrangement on the surface, however, remain unchanged even after the long-term test (Figure 6f), and also the $\Delta\lambda_{peak}$ amplitude still lies within the ±20% tolerance limit set by ISO 26142 (Figure 6e).[43] This further corroborates the very good stability and resistance to deactivation of the $Pd_{65}Au_{25}Cu_{10}$ ternary alloy system.

■ CONCLUSIONS

We have systematically assessed the optimum Au and Cu alloyant concentrations in ternary alloy PdAuCu nanoparticles to enable hysteresis-free and sensitive plasmonic hydrogen
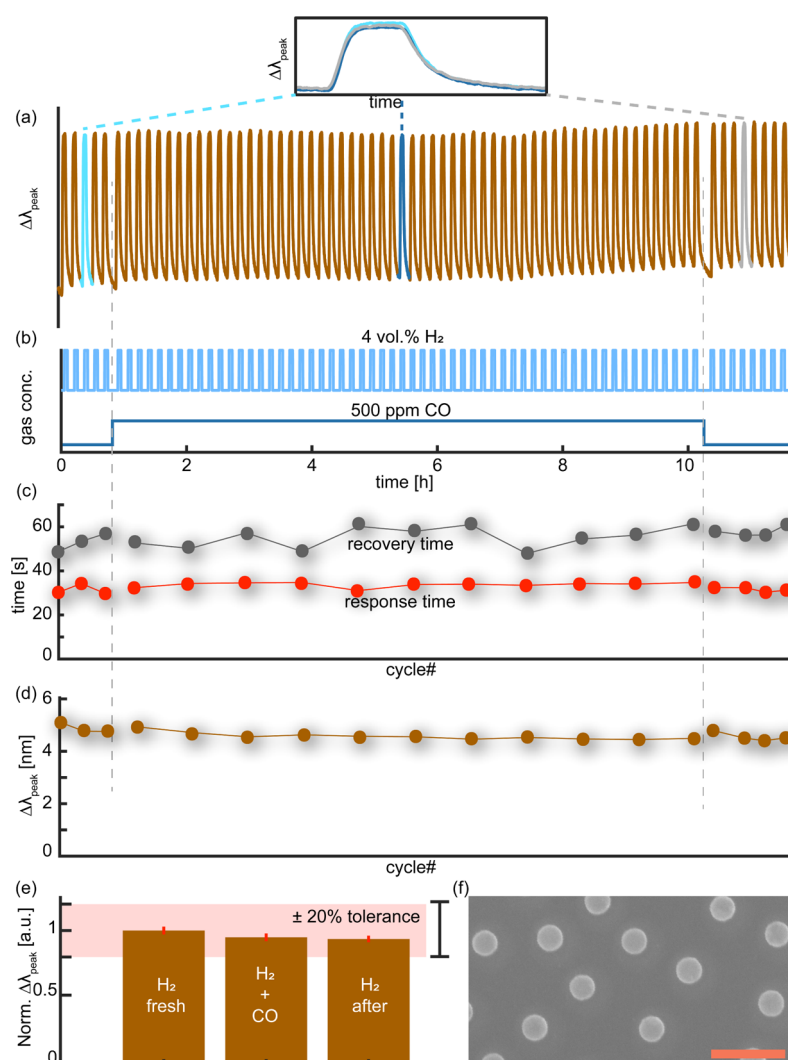
Figure 6. Long-term deactivation test of the $Pd_{65}Au_{25}Cu_{10}$ alloy system. (a) Temporal response of $\Delta\lambda_{peak}$ to 4 vol. % H_2 pulses in synthetic air at 30 °C, with and without the 500 ppm CO background, as depicted in (b). (c) Sensor response and recovery times (t_{50}), and (d) $\Delta\lambda_{peak}$ extracted for each cycle and plotted versus cycle number. (e) $\Delta\lambda_{peak}$ normalized with the response to the first hydrogen pulse for (i) the initial H_2 cycles in pure synthetic air, (ii) the H_2 cycles in the 500 ppm CO background in synthetic air, and (iii) final H_2 cycles again in pure synthetic air. The error bars correspond to standard deviation of the cycles in each category. The red band denotes the ±20% tolerance set by ISO 26142.[43] (f) SEM micrograph of the nanodisk array after the long-term deactivation test. Scale bar denotes 500 nm.

sensor operation in a CO-rich environment according to the ISO 26142 testing protocol. We have found that the minimum Cu content required to provide deactivation protection in the 500 ppm CO background in synthetic air is 10 at. % and that the required minimum amount of Cu depends on the CO concentration in the background, where a higher CO concentration requires a higher Cu content. Moreover, we observed that, in the ternary PdAuCu system, the hysteresis suppression effect is predominantly driven by the Au component and that the minimum amount of Au required for obtaining a linear, hysteresis-free, and yet sensitive response is 25 at. % Au in combination with a Cu concentration of 10 at. % < Cu < 20 at. %. Consequently, we have identified the $Pd_{65}Au_{25}Cu_{10}$ alloy as the champion system that constitutes the best compromise in terms of hysteresis-free response, sensitivity, and CO deactivation resistance. This system also exhibits very good long-term stability during operation under severe CO poisoning conditions, where it shows no sign of deactivation after more than 50 hydrogen pulses in the 500 ppm CO background after more than 12 h on stream. For

further quantitative assessment of PdAuCu ternary alloy hydrogen sensor performance in comparison to other types of hydrogen sensors, we refer to a recent review.[1] In a wider perspective, this study may provide important insights into other applications of Pd alloy systems and their hydrides, such as in hydrogen separation membrane technology or heterogeneous catalysis, where alloying is a widely employed strategy for performance optimization with respect to, for example, hydrogen permeability or the catalytic reaction rate under CO-rich conditions.

■ METHODS

Sample Fabrication. The alloy nanodisk arrays were fabricated using layer-by-layer deposition through a hole mask[16] onto 1 × 1 cm glass substrates (Borofloat, Schott Scandinavia AB). Deposition was followed by annealing at 500 °C for 24 h under a flow of 4% H_2 in Ar.[17] A more detailed description of the nanofabrication procedure can be found in our earlier work.[17]

Deactivation and Poisoning Tests. The deactivation measurements were carried out in a quartz tube flow reactor with optical

access for transmittance measurements (X1, Insplorion AB) at atmospheric pressure, using synthetic air as the carrier gas, which has a time constant for complete gas exchange of ~10 s.[44] The gas flow rate (335 mL/min) and gas composition were controlled by mass flow controllers (Bronkhorst ΔP). The sample inside the flow reactor was illuminated by white light (AvaLight-Hal, Avantes) through an optical fiber equipped with a collimating lens. The transmitted light was then analyzed using a fiber-coupled fixed-grating spectrometer (AvaSpec-1024, Avantes). The LSPR peak descriptors were obtained by fitting a 20th order polynomial to the LSPR peak in the measured optical extinction spectra. The measurement temperature was kept at 30 °C.

Pressure−$\Delta\lambda_{peak}$ Isotherm Measurements. The isotherm measurements were performed in a custom-made vacuum chamber setup with optical windows reported earlier.[7,17] The absolute hydrogen pressure in the chamber was monitored using two capacitive pressure gauges with different ranges (MKS Baratron). Optical transmittance through the sample was enabled using quartz vacuum viewports mounted on the vacuum chamber and by using a fiber-coupled, unpolarized white light source (Avantes AvaLight-Hal) and a fixed grating fiber-coupled spectrophotometer (Avantes SensLine AvaSpec-2048XL). The pressure inside the chamber was controlled using microbar-precision leak valves. The temperature was controlled with a heating coil wrapped around the chamber and a temperature controller (Eurotherm 3216N) in a feedback loop manner, where the sample surface temperature inside the vacuum chamber was continuously used as the input. We performed all of our experiments at constant 30 °C. The LSPR peak descriptors were obtained by fitting a Lorentzian to the LSPR peak in the measured optical extinction spectra.

■ AUTHOR INFORMATION

Corresponding Author
Christoph Langhammer − *Department of Physics, Chalmers University of Technology, Göteborg 412 96, Sweden;* ● orcid.org/0000-0003-2180-1379; Email: clangham@chalmers.se

Authors
Iwan Darmadi − *Department of Physics, Chalmers University of Technology, Göteborg 412 96, Sweden;* ● orcid.org/0000-0002-5921-9336
Sarah Zulfa Khairunnisa − *Department of Physics, Chalmers University of Technology, Göteborg 412 96, Sweden*
David Tomeček − *Department of Physics, Chalmers University of Technology, Göteborg 412 96, Sweden*

Complete contact information is available at:
https://pubs.acs.org/10.1021/acsanm.1c01242

Notes
The authors declare no competing financial interest.

■ ACKNOWLEDGMENTS

■ REFERENCES

(1) Darmadi, I.; Nugroho, F. A. A.; Langhammer, C. High-Performance Nanostructured Palladium-Based Hydrogen Sensors—Current Limitations and Strategies for Their Mitigation. *ACS Sens.* **2020**, *5*, 3306−3327.

(2) Wadell, C.; Syrenova, S.; Langhammer, C. Plasmonic Hydrogen Sensing with Nanostructured Metal Hydrides. *ACS Nano* **2014**, *8*, 11925−11940.

(3) Hübert, T.; Boon-Brett, L.; Black, G.; Banach, U. Hydrogen Sensors - A Review. *Sens. Actuators, B* **2011**, *157*, 329−352.

(4) Boon-Brett, L.; Bousek, J.; Black, G.; Moretto, P.; Castello, P.; Hübert, T.; Banach, U. Identifying Performance Gaps in Hydrogen Safety Sensor Technology for Automotive and Stationary Applications. *Int. J. Hydrogen Energy* **2010**, *35*, 373−384.

(5) Fisser, M.; Badcock, R. A.; Teal, P. D.; Hunze, A. Optimizing the Sensitivity of Palladium Based Hydrogen Sensors. *Sens. Actuators, B* **2018**, *259*, 10−19.

(6) Pak, Y.; Jeong, Y.; Alaal, N.; Kim, H.; Chae, J.; Min, J.-W.; Devi, A. A. S.; Mitra, S.; Lee, D. H.; Kumaresan, Y.; et al. Highly Stable and Ultrafast Hydrogen Gas Sensor Based on 15 Nm Nanogaps Switching in a Palladium−Gold Nanoribbons Array. *Adv. Mater. Interfaces* **2019**, *6*, 1801442.

(7) Wadell, C.; Nugroho, F. A. A.; Lidström, E.; Iandolo, B.; Wagner, J. B.; Langhammer, C. Hysteresis-Free Nanoplasmonic Pd-Au Alloy Hydrogen Sensors. *Nano Lett.* **2015**, *15*, 3563−3570.

(8) Hayashi, Y.; Yamazaki, H.; Masunishi, K.; Ikehashi, T.; Nakamura, N.; Kojima, A. Effects of Poisoning Gases on and Restoration of PdCuSi Metallic Glass in a Capacitive MEMS Hydrogen Sensor. *Int. J. Hydrogen Energy* **2020**, *45*, 1187−1194.

(9) Hayashi, Y.; Yamazaki, H.; Ono, D.; Masunishi, K.; Ikehashi, T. Investigation of PdCuSi Metallic Glass Film for Hysteresis-Free and Fast Response Capacitive MEMS Hydrogen Sensors. *Int. J. Hydrogen Energy* **2018**, *43*, 9438−9445.

(10) Darmadi, I.; Nugroho, F. A. A.; Kadkhodazadeh, S.; Wagner, J. B.; Langhammer, C. Rationally Designed PdAuCu Ternary Alloy Nanoparticles for Intrinsically Deactivation-Resistant Ultrafast Plasmonic Hydrogen Sensing. *ACS Sens.* **2019**, *4*, 1424−1432.

(11) Nugroho, F. A. A.; Darmadi, I.; Zhdanov, V. P.; Langhammer, C. Universal Scaling and Design Rules of Hydrogen-Induced Optical Properties in Pd and Pd-Alloy Nanoparticles. *ACS Nano* **2018**, *12*, 9903−9912.

(12) Namba, K.; Ogura, S.; Ohno, S.; Di, W.; Kato, K.; Wilde, M.; Pletikosić, I.; Pervan, P.; Milun, M.; Fukutani, K. Acceleration of Hydrogen Absorption by Palladium through Surface Alloying with Gold. *Proc. Natl. Acad. Sci. U.S.A.* **2018**, *115*, 7896−7900.

(13) Burch, R.; Buss, R. G. Absorption of Hydrogen by Palladium-Copper Alloys. Part 1—Experimental Measurements. *J. Chem. Soc., Faraday Trans. 1* **1975**, *71*, 913−921.

(14) Burch, R.; Buss, R. G. Absorption of Hydrogen by Palladium-Copper Alloys. Part 2.—Theoretical Analysis. *J. Chem. Soc., Faraday Trans. 1* **1975**, *71*, 922−929.

(15) Buttner, W.; Rivkin, C.; Burgess, R. Hydrogen Sensors. http://www.hysafe.info/wp-content/uploads/2016/07/568_RPW2014_Presentations-Research-Priorities-2014-distribution-updated-2016-05-20.pdf (accessed 17 Dec 2020).

(16) Fredriksson, H.; Alaverdyan, Y.; Dmitriev, A.; Langhammer, C.; Sutherland, D. S.; Zäch, M.; Kasemo, B. Hole−Mask Colloidal Lithography. *Adv. Mater.* **2007**, *19*, 4297−4302.

(17) Nugroho, F. A. A.; Iandolo, B.; Wagner, J. B.; Langhammer, C. Bottom-Up Nanofabrication of Supported Noble Metal Alloy Nanoparticle Arrays for Plasmonics. *ACS Nano* **2016**, *10*, 2871−2879.

(18) Dahlin, A. B.; Tegenfeldt, J. O.; Höök, F. Improving the Instrumental Resolution of Sensors Based on Localized Surface Plasmon Resonance. *Anal. Chem.* **2006**, *78*, 4416−4423.

(19) Chorkendorff, I.; Niemantsverdriet, J. W. *Concepts of Modern Catalysis and Kinetics*; Wiley, 2003.

(20) Gorodetskii, V. V.; Matveev, A. V.; Podgornov, E. A.; Zaera, F. Study of the Low-Temperature Reaction between CO and O2 over Pd and Pt Surfaces. *Top. Catal.* **2005**, *32*, 17−28.

(21) Debauge, Y.; Abon, M.; Bertolini, J. C.; Massardier, J.; Rochefort, A. Synergistic Alloying Behaviour of Pd50Cu50 Single

Crystals upon Adsorption and Co-Adsorption of CO and NO. *Appl. Surf. Sci.* **1995**, *90*, 15−27.

(22) Rochefort, A.; Fournier, R. Quantum Chemical Study of CO and NO Bonding to Pd2, Cu2, and PdCu. *J. Phys. Chem.* **1996**, *100*, 13506−13513.

(23) Illas, F.; López, N.; Ricart, J. M.; Clotet, A.; Conesa, J. C.; Fernández-García, M. Interaction of CO and NO with PdCu(111) Surfaces. *J. Phys. Chem. B* **1998**, *102*, 8017−8023.

(24) Sakong, S.; Mosch, C.; Groß, A. CO Adsorption on Cu-Pd Alloy Surfaces: Ligand versus Ensemble Effects. *Phys. Chem. Chem. Phys.* **2007**, *9*, 2216−2225.

(25) Ma, Y.; Diemant, T.; Bansmann, J.; Behm, R. J. The Interaction of CO with PdAg/Pd(111) Surface Alloys—A Case Study of Ensemble Effects on a Bimetallic Surface. *Phys. Chem. Chem. Phys.* **2011**, *13*, 10741−10754.

(26) Mezey, L. Z.; Hofer, W.; Varga, P.; Giber, J. The Drastic Effect of Oxygen on Surface Segregation. *Surf. Interface Anal.* **1990**, *16*, 520−525.

(27) Ekborg-Tanner, P.; Erhart, P. Hydrogen-Driven Surface Segregation in Pd Alloys from Atomic-Scale Simulations. *J. Phys. Chem. C* **2021**, *125* (31), 17248−17260.

(28) Kamakoti, P.; Morreale, B. D.; Ciocco, M. V.; Howard, B. H.; Killmeyer, R. P.; Cugini, A. V.; Sholl, D. S. Prediction of Hydrogen Flux through Sulfur-Tolerant Binary Alloy Membranes. *Science (80-.)* **2005**, *307*, 569−573.

(29) Morreale, B.; Ciocco, M. V.; Howard, B. H.; Killmeyer, R. P.; Cugini, A. V.; Enick, R. M. Effect of Hydrogen-Sulfide on the Hydrogen Permeance of Palladium-Copper Alloys at Elevated Temperatures. *J. Membr. Sci.* **2004**, *241*, 219−224.

(30) Conrad, H.; Ertl, G.; Latta, E. E. Adsorption of Hydrogen on Palladium Single Crystal Surfaces. *Surf. Sci.* **1974**, *41*, 435−446.

(31) He, J.-W.; Harrington, D. A.; Griffiths, K.; Norton, P. R. The Interaction of Hydrogen with a Pd(100) Surface. *Surf. Sci.* **1988**, *198*, 413−430.

(32) Langhammer, C.; Zhdanov, V. P.; Zorić, I.; Kasemo, B. Size-Dependent Kinetics of Hydriding and Dehydriding of Pd Nanoparticles. *Phys. Rev. Lett.* **2010**, *104*, 135502.

(33) Darmadi, I.; Stolaś, A.; Östergren, I.; Berke, B.; Nugroho, F. A. A.; Minelli, M.; Lerch, S.; Tanyeli, I.; Lund, A.; Andersson, O.; et al. Bulk-Processed Pd Nanocube−Poly(Methyl Methacrylate) Nanocomposites as Plasmonic Plastics for Hydrogen Sensing. *ACS Appl. Nano Mater.* **2020**, *3*, 8438−8445.

(34) Palmisano, V.; Boon-Brett, L.; Bonato, C.; Harskamp, F.; Buttner, W. J.; Post, M. B.; Burgess, R.; Rivkin, C. Evaluation of Selectivity of Commercial Hydrogen Sensors. *Int. J. Hydrogen Energy* **2014**, *39*, 20491−20496.

(35) Westerwaal, R. J.; Rooijmans, J. S. A.; Leclercq, L.; Gheorghe, D. G.; Radeva, T.; Mooij, L.; Mak, T.; Polak, L.; Slaman, M.; Dam, B.; et al. Nanostructured Pd−Au Based Fiber Optic Sensors for Probing Hydrogen Concentrations in Gas Mixtures. *Int. J. Hydrogen Energy* **2013**, *38*, 4201−4212.

(36) Rahm, J. M.; Löfgren, J.; Fransson, E.; Erhart, P. A tale of two phase diagrams: Interplay of ordering and hydrogen uptake in Pd-Au-H. *Acta Mater.* **2021**, *211*, 116893.

(37) Okamoto, H.; Massalski, T. B. The Au−Pd (Gold-Palladium) System. *Bull. Alloy Phase Diagrams* **1985**, *6*, 229−235.

(38) Subramanian, P. R.; Laughlin, D. E. Cu-Pd (Copper-Palladium). *J. Phase Equil.* **1991**, *12*, 231−243.

(39) Løvvik, O. M. Surface Segregation in Palladium Based Alloys from Density-Functional Calculations. *Surf. Sci.* **2005**, *583*, 100−106.

(40) Zhao, M.; Sloof, W. G.; Böttger, A. J. Modelling of Surface Segregation for Palladium Alloys in Vacuum and Gas Environments. *Int. J. Hydrogen Energy* **2018**, *43*, 2212−2223.

(41) Zhao, M.; Brouwer, J. C.; Sloof, W. G.; Böttger, A. J. Surface Segregation of Pd−Cu Alloy in Various Gas Atmospheres. *Int. J. Hydrogen Energy* **2020**, *45*, 21567−21572.

(42) Kim, H. Y.; Henkelman, G. CO Adsorption-Driven Surface Segregation of Pd on Au/Pd Bimetallic Surfaces: Role of Defects and Effect on CO Oxidation. *ACS Catal.* **2013**, *3*, 2541−2546.

(43) *ISO 26142:2010 Hydrogen Detection Apparatus -- Stationary Applications*; 2010.

(44) Nugroho, F. A. A.; Diaz de Zerio Mendaza, A.; Lindqvist, C.; Antosiewicz, T. J.; Müller, C.; Langhammer, C. Plasmonic Nanospectroscopy for Thermal Analysis of Organic Semiconductor Thin Films. *Anal. Chem.* **2017**, *89*, 2575−2582.